IOSR Journal of Engineering (IOSRJEN) **www.iosrjen.org**
ISSN (e): 2250-3021, ISSN (p): 2278-8719
Vol. 04, Issue 10 (October. 2014), ||V1|| PP 11-19

Optimization of Wind Duct Geometry for Maximizing Power Generation of Ducted Vertical Turbines

Taher G. Abu-El-Yazied [1], Ahmad M. Ali[1], Osama A. Montasser[2]
[1]*Design and Production, Faculty of Engineering/ Ain Shams University, Egypt*
taher_abuelyazied@eng.asu.edu.eg
[2]*Mechanical Power Engineering, Faculty of Engineering/ Ain Shams University, Egypt, On leave to join the British University in Egypt, BUE*
osama.montasser@bue.edu.eg

Abstract *This paper investigates the possibility of augmenting the power output of a ducted vertical wind turbine. The geometrical parameters of the utilized duct and the relative position of its throat to the ducted turbine center are optimize. Optimization process carried out using the Genetic Algorithm, GA, keeping into account the size and cost constraints. Two dimensional Computational fluid dynamics CFD analysis have been performed on a straight-bladed Darrieus-type vertical rotor wind turbine. CFD solver is used to compute the power coefficient, C_p, the dimensionless form of power output of a three bladed rotor wind turbine as a function of the wind free stream velocity, V, and the rotor's rotational speed, ω. Results of the CFD computational analysis for C_p are used to feed the GA with the information required to optimize the duct geometry. The new duct, optimized in this study, reduces the torque variation over a complete rotational cycle, by appropriately directing the wind air flow upstream and downstream the ducted turbine, and thus increases the turbine power conversion. The present study showed that the optimized duct geometry is of 20° convergence angle with its throat lie at the ducted turbine center. A comparison between the optimized ducted turbine and the un-ducted turbine shows that, the tip speed ratio, TSR, λ, at which the maximum power occurs, is increased from 2.62 to 3.29, the minimum torque ripple factor, TRF, is decreased from 1.691 to 0.239, and the maximum power coefficient, $C_{p,}$ is increased from 0.31 to 0.69.*

I. ***Keywords:*** *Genetic Algorithm, Maximizing wind power generation, Optimized ducted wind turbines, Optimum Wind duct geometry, Power Optimization.*

I. Introduction

It is well-known that wind energy is very important as it is one of the available clean energy resources. Rotors of the wind turbines play the most important rule in the wind energy generation. There are two different physical principles to extract power from wind. The first of them is using the airfoil drag forces, while the second is using the airfoil lift forces. The Darrieus turbine is the most common Vertical Axis Wind Turbine, VAWT, invented in 1931 [1, 8]. On the basis of the lift force principle, a lot of investigations aim to improve the performance of vertical axis wind turbines by augmenting the wind velocity. Contrary to that the horizontal axis wind turbine is popular for large scale power generation; the vertical axis wind turbine is utilized for small scale power generation [6, 9].

Ducting the vertical axis wind turbines to augment their output power was studied by [2, 3]. In the present study, a new duct design is proposed, for a given turbine design, and optimized to reduce the variation in torque over a complete rotational cycle by appropriately directing the flow upstream and downstream the turbine, and thus increasing power conversion. The new duct geometrical parameters and the turbine center relative position to its throat were optimized to augment the power generation of the ducted wind turbine. The optimization process utilized the Genetic Algorithm, GA, package supplied with information for the generated power of the ducted turbine computed with a CFD solver.

The present paper is organized as follows. In the following section, the optimization plan, of the present turbine duct geometry to maximize the turbine generated power has been introduced. The CFD numerical solution carried out in the present study is outlined in the same section. In this section, steps of the present optimization methodology are listed as well. The optimized duct configurations and the duct geometry optimization parameters are also overviewed. The study results are viewed and discussed in the next section. Conclusions of the present study are summarized in the last section.

II. Optimization Plan of the Present Duct Geometry

Genetic Algorithm, GA, is the most popular type of Evolutionary Algorithms, EA, [7]. A fully automated optimization process takes place using CFD analysis coupled to the GA. The modeFRONTIER

commercial program, the commercial tool Gambit, and the industrial CFD ANSYS-Fluent code are coupled. ModeFRONTIER is a decision-maker program to be used for evaluating the investigated configurations. Gambit is a commercial tool for geometry and grid generation with quality check included. The industrial CFD ANSYS-Fluent code is used to compute the flow field around the turbines though it is ducted or not.

As a result of the CFD computation, the objective functions are determined, and stored in a result file. The optimization procedure is automated using journal scripts to restart Gambit, Fluent and the commercial program modeFRONTIER and calling all codes in the right sequence as shown in Fig. 1, below. By checking the values stored in the result file, Multi Objective Genetic Algorithm (MOGA) is able to decide how to modify the input parameters before starting a new geometry generation. First generation of the input parameters is generated by using design of experiments based on a pseudo random called Sobol sequence. Both MOGA and Sobol are integrated algorithms inside modeFRONTIER program. The optimization parameters were chosen according to [10].

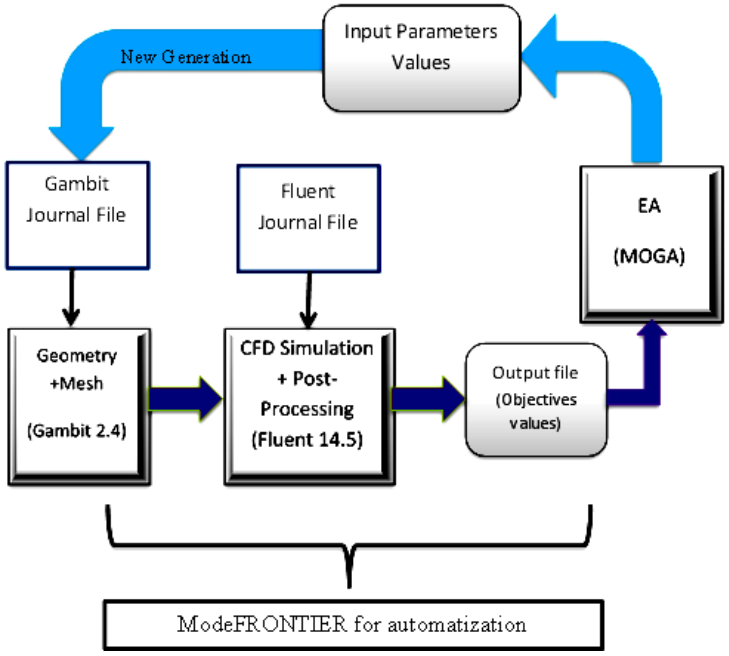

Figure 1 Schematic description of MOGA optimizer and CFD code coupled by modeFRONTIER

2.1. CFD Numerical Solution

Aerodynamics numerical analysis carried out in this study is detailed in another study of the present work authors [4]. We will concentrate here on what is different than that done there in [4], regarding the new configurations of the present ducted turbine and the duct geometry optimization as well.

The optimization flow objective parameters are chosen as follows:

1- The speed ratio, λ, defined as:

$$\boldsymbol{\lambda = \frac{R\omega}{V}} \qquad 1$$

2- The power coefficient, C_p, defined as:

$$\boldsymbol{C_p = \frac{P_{mech}}{\frac{1}{2}\rho A V^3}} \qquad 2$$

3- Torque ripple factor, *TRF*, is expressed as:

$$\boldsymbol{TRF = \frac{T_{Pk-Pk}}{\bar{T}}} \qquad 3$$

Where: *R*, is rotor radius, ω is the rotational angular speed, *V*, is the wind free stream velocity, P_{mech} is the generated mechanical power, ρ, is the wind air density, *A*, is the rotor projected area, and, T_{pk_pk} is the peak-to-peak amplitude of the instantaneous torque, and $\bar{T}$ is the torque averaged over a complete rotational cycle. Torque ripple factor, *TRF*, gives a dimensionless quantity representative of the variation in torque that can be universally compared across various turbines. When the torque produced is almost steady, the value of the ripple factor approaching 1.

Simulations were carried out for both ducted and un-ducted turbine geometries. Details of the turbine chosen for the CFD simulation in this study are given in table 1 below. This turbine was adopted from the the numerically investigation by [4, and 5] and experimental work by [11].

Table 1 Dimensions of the turbine used in the present study

Rotor diameter, *D*, mm	1030
Rotor blade height, *H*, mm	1414
Number of blades, *n*	3
Blade profile	NACA 0021
Turbine swept area, A_s , m^2	1.236
Blade Chord length, *C*, mm	85.8
Solidity σ	0.25

2.1.1. Description of the numerical flow field

Three separate zones are created, rotor zone being rotary, square far-field being stationary and shaft field being stationary as shown in Fig. 2 below. The far-field mesh which is of hexahedral type is less dense as compared to hexahedral mesh in the rotary zone. Inlet was set as a velocity inlet, with a constant velocity profile of 9 m/s, while outlet was set as a pressure outlet. Two symmetry boundary conditions were used for the two side walls.

The appropriate size of the computational domain has been investigated in this study. The computational domain is of increasing dimensions, square domain of size, suitably normalized by the rotor radius R. The ratio between the square domain length and the rotor radius is shown in Fig. 2.

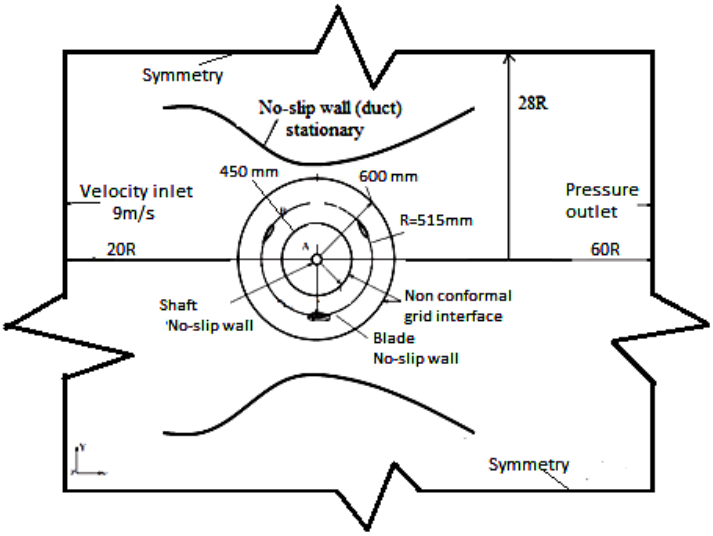

Figure 2 Schematic of the computational domain

2.1.2. Main features OF THE NUMERICAL simulation

A complete campaign of simulations, based on full RANS unsteady calculations, was performed for a three bladed rotor architecture characterized by a NACA 0021 airfoil. The tip speed ratio, λ, was varied from a value of λ = 1.44, corresponds to an angular velocity of ω = 25.1 rad/s, to λ = 3.8, corresponds to ω = 66.41rad/s. The wind air dynamic viscosity was assumed to be $1.78 \cdot 10^{-5}$ Pa·s, the density was set to 1.225 kg/m^3. Computations were done for air free stream velocity, *V*, value of 9 m/s.

The realizable *k-ε* turbulence model is usually recommended for rotating bodies. This model usually provides improved results for swirling flows and flow pattern involving separation when compared to the standard *k-ε* model. The near-wall treatment relies on standard wall functions. The present study involves the application of SIMPLE scheme. Among several discretization special schemes available in FLUENT, Least squares cell based gradient with standard pressure and second order upwind scheme are found to be appropriate for the present study. Simulation utilizes the second order implicit transient formulation was used as the most suitable one for the present study. Convergence criterion for the solution is set as 10^{-5}. Currently, our area of

consideration is to determine the forces acting on each of the three rotating airfoils and to obtain an optimum value of tip speed ratio which gives the maximum power output when wind approaching the turbine at a speed of 9 m/s.

The aerodynamics model was solved using commercial CFD-Fluent solver which solves Navier-Stokes equations using finite volume technique. Details of the used numerical models and solver strategies adopted are given in [4]. Ten complete revolutions are often computed for each tip speed ratio, using a calculated time-step. The first revolutions is used to initiate the correct flow solution, while the flow properties, in particular the power coefficient C_p, are obtained by averaging the results during the last two computational revolutions.

2.2. Optimization Methodology

The following steps represent the optimization methodology of the present work:

1. Identifying the physical quantity to be maximized as the velocity inside the duct.
2. Create Gambit journal file to generate duct shape geometry by seven curvature points, as shown in Fig. 3 below, and define the boundary conditions as shown in Fig. 2 above. Two-dimensional computational mesh domain, consequently formed by Gambit after determining the sensitivity of the domain size, extends with respect to R, rotor radius, for the un-ducted and ducted turbine cases.
3. Identifying the input parameters for Gambit as the *x* and *y* coordinates of each of the seven curvature points of the duct, as shown in Fig. 3 below.
4. Create the Fluent journal file to solve a steady state solution for the proposed duct, without turbine, the output of which is the velocity inside the duct for a specific duct position.
5. Identifying the velocity maximized duct positions, as the three positions shown in Fig. 4 below. The optimization process will take place at each of these positions.
6. Perform optimization loop, presented in Fig. 1 above, for B, A, and C optimized duct positions shown in Fig. 4.
7. Generate mesh for the turbine ducted by the optimum duct geometry obtained by the optimization process, mentioned in step 6 above, and identify new boundary conditions as presented in Fig. 2 above.
8. Solve the transient CFD problem for the optimum ducted turbine, obtained in step 7 above, and draw the power coefficient, C_p, obtained for different λ values.
9. Repeat steps 7 and 8 above for each of the optimized duct position specified as shown in Fig. 4.
10. Compare between the C_p results for all the optimized duct positions.

Fig. 3 shows the configuration parameters used to optimize the duct shape. The duct geometry is generated by seven curvature points, the *x* and *y* coordinates of which are configured as shown in the figure. The curvature points *y* coordinates of the duct throat is fixed at ± 0.65 m while the *x* coordinate of the duct throat center is fixed at -0.65 m, 0, and +0.65 m for A, B, and C optimized duct positions respectively. The duct length, *x* distance between *a* and *g* duct curvature points is fixed at 2.15 m so that *x* coordinates of *a* and *g* points are fixed at -1.15 m and +1.0 m respectively, noting that *x* value is increased in the air flow direction.

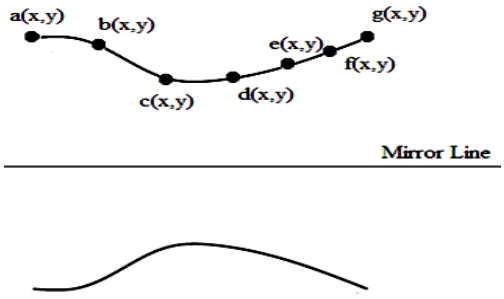

Figure 3 Schematic description of the free optimization parameters characterizing a duct shape, a_y , b_x , b_y , c_x , c_y , d_x , d_y , e_x , e_y , f_x , f_y , *and* g_y

Fig. 4, below, shows configurations of the velocity maximized positions inside the duct, B, A, and C. The duct shape is optimized according to these chosen position configurations. For position B, the duct throat line lies at the turbine center, while for positions A, and C, the duct throat line lies at a distance, 0.65 m, downstream and upstream the turbine center respectively.

Schematic description of the optimization parameters used to modify the duct shape at position B is shown in Fig. 5 below. *X* and *y* coordinates of the turbine center are fixed at (0, 0), 1.15 m downstream and 1.0

m upstream the duct ends, as shown in the figure. *X* and *y* Coordinates of the curvature points of the duct throat diameter are fixed at (0, ± 0.65 m) for position B configuration. For positions A and C, the duct throat diameter points coordinates are fixed at (0.65, ± 0.65 m) and (-0.65, ± 0.65 m) respectively, where values of *x* axis increases in the flow direction.

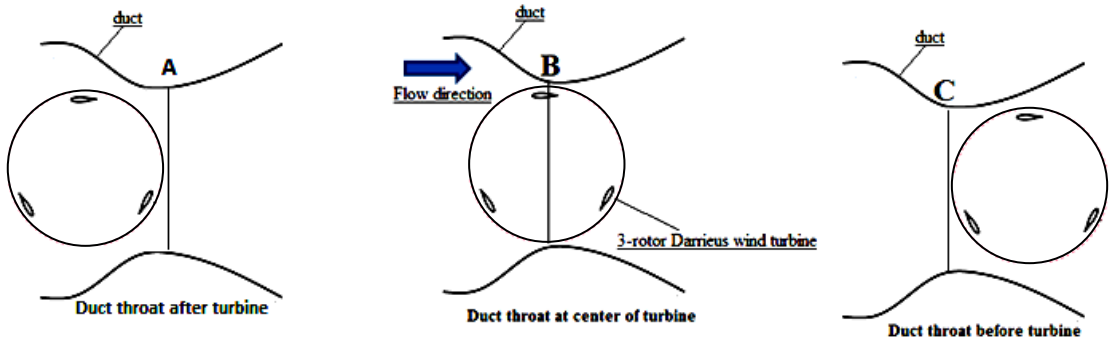

Figure 4 Maximized velocity positions, according to which the duct shape is optimized

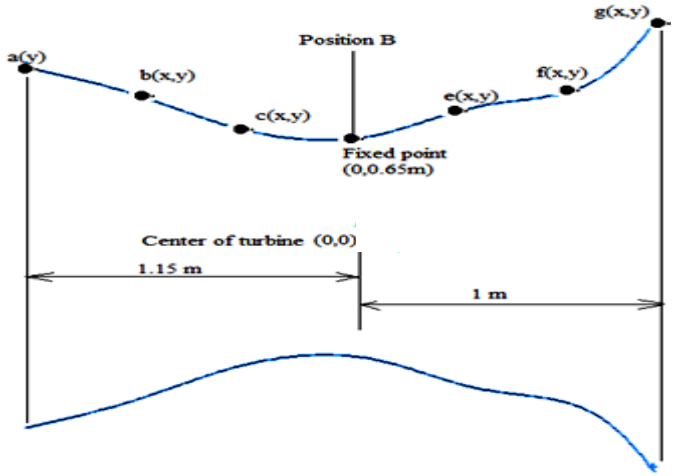

Figure 5 Schematic description of the free optimization parameters used to modify the duct shape at position B

III. RESULTS AND DISCUSSION

3.1 Power Coefficient, *CP* and Torque Ripple Factor, *TRF*, Results

Results of the present CFD simulation for C_p, the present optimized target function, are verified as shown in Fig. 6, below. The present results give a good agreement with experimental results published by [11] for a same Darrieus turbine configuration. Similar tendency to the numerical CFD results of [5], is observed as well.

Numerical results for the power performance, C_p, of the turbine un-ducted and ducted with the three optimized duct positions are shown in Fig. 6, below, for different values of tip speed ration, λ.

Fig. 6 shows that the maximum C_p obtained for the turbine ducted with optimized position B. The peak point is for C_p equal to 0.69 at λ value equal to 3.29. Velocity and Pressure distributions are numerically determined for the turbine ducted with the three optimized duct positions. Obtained distribution results verified that the velocity is most maximized with the B position duct configuration. .

Torque ripple factor results, *TRF* (3), of the turbine un-ducted and ducted with the three optimized duct positions are shown in Fig. 7, below, for different *TSR*, λ, values. The figure shows that the minimum *TFR* values occurred at ducted turbine ducted with A and B optimized duct positions. The minimum *TRF* value, observed for the B duct position, is equal to 0.239 at λ equal to 3.29 compared to the *TRF* minimum value of the un-ducted turbine of 1.69 at λ equal to 2.62 as shown in the figure.

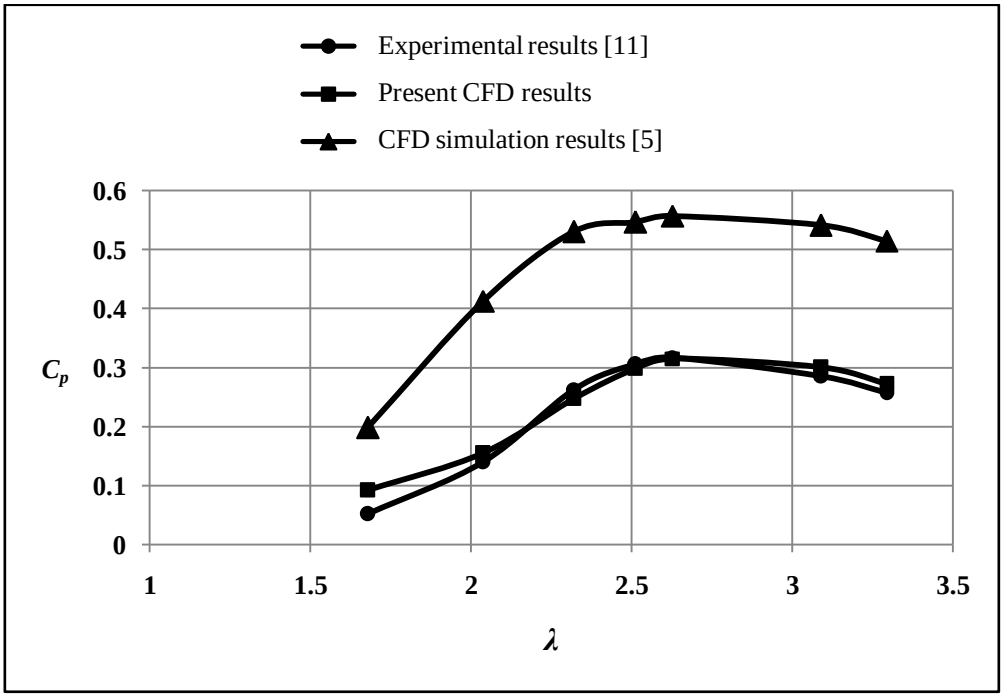

Figure 5 Verification of the present CFD model, compared to published experimental and CFD results for a Darrieus turbine [5, 11]

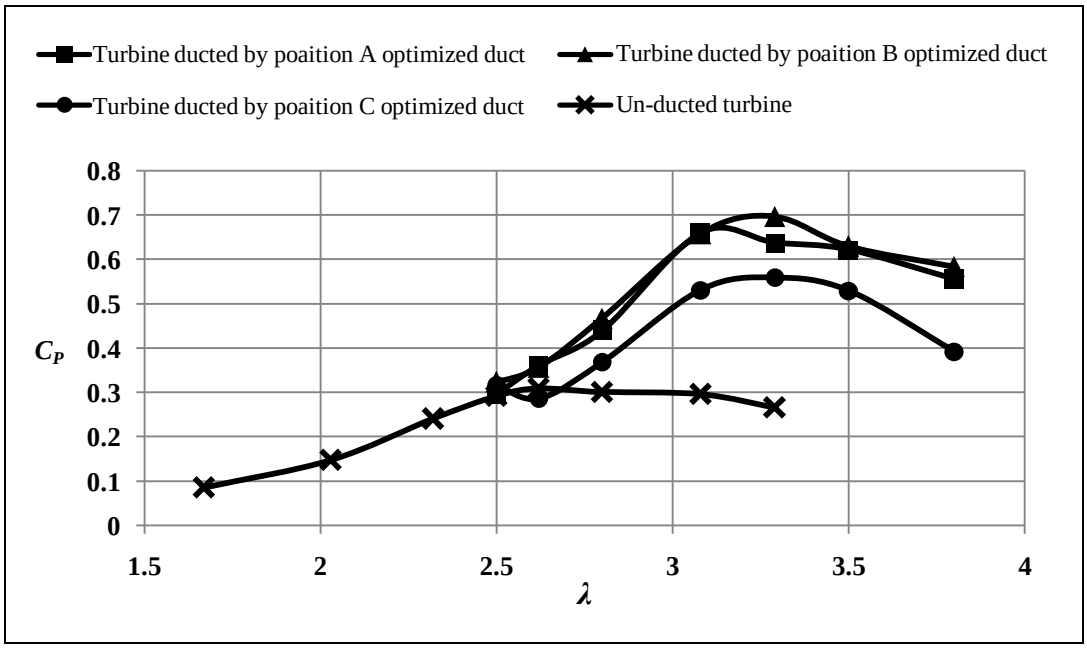

Figure 6 Power coefficient results for the turbine ducted with the three optimized duct positions

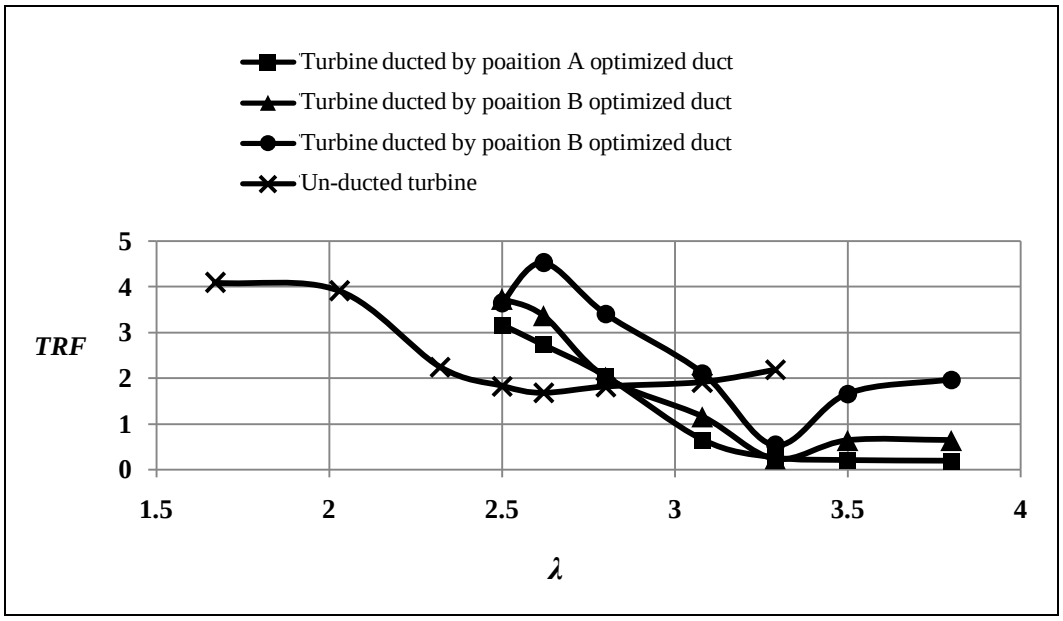

Figure 7 Comparison for the *TRF* results of turbine, un-ducted and ducted with the optimized duct positions

3.2 Space utilization with using ducted wind turbine

To discuss the performance of ducted turbine in utilizing the turbine configuration space, a comparison between the simulation results of the turbine, ducted with the most optimized duct position, B, and un-ducted turbine with single and doubled rotor diameters is shown in Figs. 8 and 9 below. Fig. 8 shows the power coefficient, C_p, results for different *TSR*, λ, values. The figure shows that the maximum power coefficient occurs with the optimized ducted turbine, C_p = 0.69 at λ = 3.29, compared to the un-ducted turbine of single rotor diameter, C_p = 0.312 at λ = 2.61, and that of doubled rotor diameter, C_p = 0.36 at λ = 2.81.

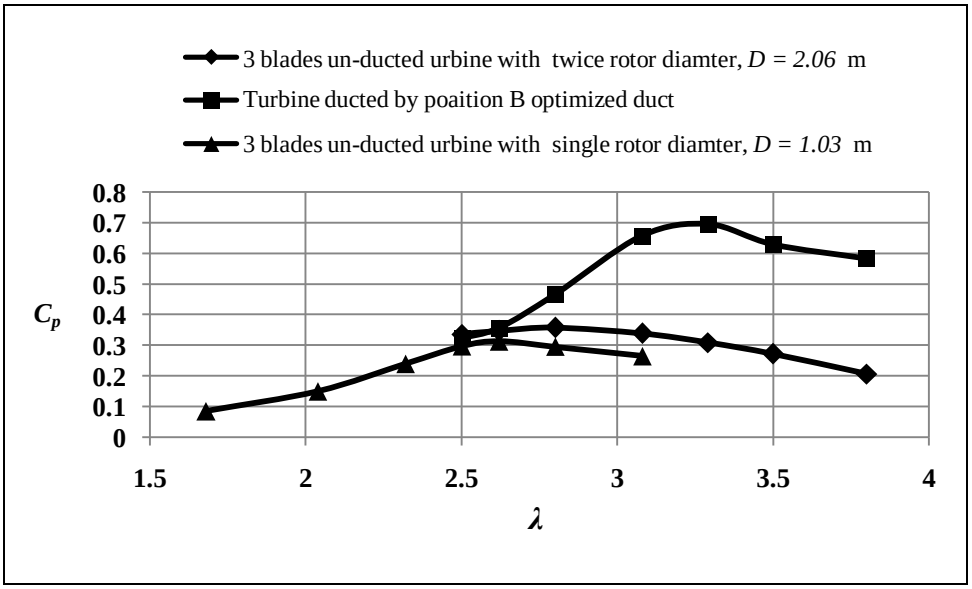

Figure 8 Comparison of power coefficient results between un-ducted turbines of single and twice rotor diameter, and the optimized ducted turbine for V = 9 m/s

The C_p value is not an indication for the generated mechanical power value since the power is proportional to both C_p and the rotor projected area, or the rotor diameter, as well. The absolute power value is calculated and presented in Fig. 9 below. The figure shows that in case of the optimized ducted and twice diameter un-ducted turbines, the absolute generated power value is very close to each other equal to about 450 W. The power value of the single diameter un-ducted turbine is shown to be relatively very small of value equal to about 200 W.

It therefore, to get about the same generated power value, one should use two of un-ducted turbine of the same rotor diameter or one un-ducted turbine of twice rotor diameter instead of using one optimized ducted turbine. This means that un-ducted turbines need a large configuration space and thus turbine ducting most utilize the available offered space.

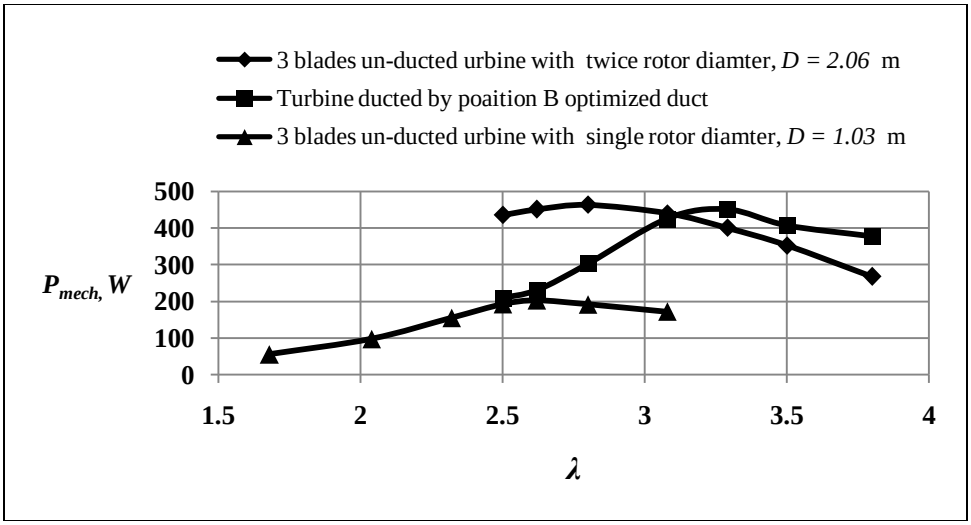

Figure 9 Comparison of mechanical power of un-ducted turbines of single and twice rotor diameter, and the optimized ducted turbine for $V = 9$ m/s

IV. CONCLUSIONS

A duct configuration is proposed and optimized in this study to be used with Darrieus vertical axis wind turbine for maximizing the output generated power. The effect of ducting a three bladed rotor Darrieus-type vertical axis wind turbine is simulated using a CFD solver. The Genetic Algorithm, GA, supplied with the results of the CFD solver for the turbine output power, was used to optimize the geometrical parameters of the duct along with deciding the optimum relative position of its throat to the ducted turbine center. This is done while keeping into account the size and cost constraints. The main conclusions from this study are summarized as follows:

1. Convergence angle of the optimized duct was found to be equal to 20^o.
2. Optimum duct-turbine relative position was found to be as such that, the turbine center coincides with the throat of the duct.

   A comparison with an un-ducted turbine, the optimized ducting of the turbine results in:
3. The tip speed ratio, *TSR*, at which the maximum power results occurs, is increased from 2.62, $\omega = 45.73$ rad/s, to 3.29, $\omega = 57.42$ rad/s.
4. The maximum power coefficient, C_p, is increased from 0.239 to 0.69.
5. The minimum torque ripple factor, *TRF*, is decreased from 1.691 to 0.239.
6. The present study shows that, one should use two units of un-ducted turbine of the same rotor diameter or one un-ducted turbine of twice rotor diameter instead of using one optimized ducted turbine to get about the same generated power value. This means that un-ducted turbines need a large configuration space and thus turbine ducting most utilizes the available offered space.

REFERENCES

Proceedings Papers:

[1] W.J. Book, Modelling design and control of flexible manipulator arms: A tutorial review, *Proc. 29th IEEE Conf. on Decision and Control*, San Francisco, CA, 1990, 500-506.

Journal Papers:

[1] T. J. Price, UK large-scale wind power programme from 1970 to 1990: the Carmarthen Bay experiments and the musgrove vertical-axis turbines, *Wind Engineering, vol. 30*, 2006, 225-242.

[2] R. A. Kishore, T. Coudron, and S. Priya, Small-scale wind energy portable turbine (SWEPT), *Journal of Wind Engineering and Industrial Aerodynamics, vol. 116*, 2013, 21-31.

[3] A. Malipeddi and D. Chatterjee, Influence of duct geometry on the performance of Darrieus hydroturbine, *Renewable Energy, vol. 43*, 2012, 292-300.

[4] H. N. Doghiem, Taher G. Abu-El-Yazied, Ahmad M. Ali and Islam M. Hassan, Investigation of the Aerodynamic Performance of Darrieus Vertical Axis Wind Turbine, *IOSR Journal of Engineering, IOSRJEN, vol. 04*, 2014, 18-29.

[5] M. Raciti Castelli, A. Englaro, and E. Benini, The Darrieus wind turbine: Proposal for a new performance prediction model based on CFD, *Energy, vol. 36*, 2011, 4919-4934.

Books:

[6] I. Paraschivoiu, *Wind turbine design: with emphasis on Darrieus concept* (Presses inter Polytechnique, 2002).

[7] S. Sivanandam and S. Deepa, *Genetic algorithm optimization problems* (Springer, 2008).

Theses:

[8] M. H. A. Mohamed, *Design optimization of savonius and wells turbines*, Ottovon-Guericke University Magdeburg, 2011.

Proceedings Papers:

[9] S. Li and Y. Li, Numerical study on the performance effect of solidity on the straight-bladed vertical axis wind turbine, *Power and Energy Engineering Conference (APPEEC), 2010 Asia-Pacific*, 2010, 1-4.

[10] A. Mosavi, Multiobjective Optimization of Spline Curves Using Mode Frontier, in *Proceedings of International modeFRONTIER Users' Meeting*, 2010.

[11] M. R. Castelli, G. Ardizzon, L. Battisti, E. Benini, and G. Pavesi, Modeling strategy and numerical validation for a Darrieus vertical axis micro-wind turbine, in *ASME 2010 International Mechanical Engineering Congress and Exposition*, 2010, 409-418.

Appendix

A	rotor projected area, $D*H$, m^2	R	rotor radius, m
C	blade chord length, m	*TRF*	torque ripple factor
CFD	computational fluid dynamics	$T_{pk\text{-}pk}$	peak to peak instantaneous torque, Nm
C_p	power coefficient	V	wind velocity at the computational domain entrance, m/s
D	rotor diameter, m	VAWT	vertical axis wind turbine
EA	evolutionary algorithms	λ	*TSR*, tip-speed ratio
GA	genetic algorithms	μ	wind air viscosity, kg/ms
H	rotor blade height, m	ρ	wind air density, kg/m^3
MOGA	multi objective genetic algorithm	σ	solidity factor
n	number of blades	ω	rotor angular rotational speed, 1/s
P_{mech}	output mechanical power, W		